19th Brazilian Congress of Thermal Sciences and Engineering
November 06th-10th, 2022, Bento Gonçalves - RS - Brazil

ENC-2022-0486
ANALYSIS OF SINGLE-BUBBLE DYNAMICS IN CONFINED CHANNELS

Thiago Sirino
Ernesto Mancilla
Multiphase Flow Research Center (NUEM), Federal Technological University of Paraná (UTFPR)- Rua Deputado Heitor Alencar Furtado 5000, Bloco N, CEP 81280-340, Curitiba, Brasil
e-mails: thiagosirino@hotmail.com; faermara@hotmail.com
Rigoberto E. M. Morales
Multiphase Flow Research Center (NUEM), Federal Technological University of Paraná (UTFPR)- Rua Deputado Heitor Alencar Furtado 5000, Bloco N, CEP 81280-340, Curitiba, Brasil
e-mail: rmorales@utfpr.edu.br

Abstract. *In this work, the effect of the confinement direction on the dynamics of single bubbles rising through a vertical water channel was investigated by using the shadowgraph technique. Three different sets of bubble sizes, with diameters between 1.32 to 3.06 mm, were released in the bottom of a glass tank filled with water. The channel was equipped with moving glass sheets and glass stripes that were used to obtain different tank cross sectional geometry. The range of confinement degree, defined as the ratio of bubble diameter (D) to channel hydraulic diameter (Dh) was varied between 0.13 to 0.98. Bubble shape, terminal velocity and drag coefficient were analyzed. The aspects ratios even for the less confined channel presented a decrease when compared to an unconfined system. The terminal velocity decrease not only depends on the hydraulic diameter but also the confinement direction and bubble size. Also, the walls proximity is responsible to a drag increase especially due the energy loss due to collisions and higher shear stresses in the thin film between the bubble surface and the walls.*

Keywords: *single bubbles, confinement direction, shape, velocity, drag coefficient*

1. INTRODUCTION

The rising of bubbles is very common in many industrial processes, and it is a complex topic in multiphase flow due the variety of variables that influence the bubble dynamics. The majority of the studies found in literature correspond to bubbles rising in non-confined systems (Tomiyama et al., 2002, Celata et al., 2007 Cano-Lozano et al., 2013, Premlata et al., 2015, Tripathi et al., 2015, Cano-Lozano, et al., 2016, Sharaf et al., 2017).

On the other hand, most studies involving bubbles flowing in between two walls (confined systems) concern to Hele-Shaw cells. In these cases, the bubbles are flattened between the walls, and then their movements are restricted to a two-dimensional plane. Thus, their dynamic becomes governed by inertial effects and viscous friction at the wall (Drews et al. 2009, Böhm et al. 2014, Filella et al. 2015).

Regarding works where the bubbles was not flattened, Figueroa-Espinoza et al. (2008) presented a drag coefficient model valid for bubbles rising in silicon oils as function of the confinement parameter s (s=a/W, where a is the bubble radius and W is the wall-to-wall distance). Also, Kumar and Vanka (2015) analyzed numerically the effects of confinement in a square duct with three confinement ratios (CR = 2, 3 and 4), defined as the ratio of duct width to bubble diameter. Morton numbers of 0.001 and 0.01 and Eötvös numbers of 1, 10, 50 and 100 were evaluated. The authors observed that as the Eötvös number increased the aspect ratio also increased, while by the increase in Morton number and in the confinement, the aspect ratio decreased. Additionally, the velocity variation was not linear with the confinement ratio. Soltani et al. (2018) investigated the flow of air bubbles in a water- glycerol solution co-flow through a rectangular channel (3x5.8 mm). They proposed a model for the terminal velocity in the creeping flow regime (Re<1). They attributed the velocity discrepancies between bubbles rising in a tube and rectangular channel to the asymmetric flow around them caused by the channel corners. Not many studies have explored in detail the influence of the confinement direction.

Therefore, in this work, experimental measurements of single bubbles rising in quiescent deionized water in a rectangular domain with variable dimensions in both directions were carried out. The bubbles are in the surface tension regime (i.e., between 1.32 to 3.06 mm in diameter). The confinement parameter was defined as D/Dh, in which D is the bubble diameter and Dh is the hydraulic diameter of the channel, defined as Dh=4A/P where A is the channel area and P the channel perimeter. The results were compared with the correlations found in the literature.

2. METHODOLOGY

The experimental setup employed in this study is illustrated in Fig. 1. It consists of a rectangular glass tank with 700 mm in height, 80 mm in depth and 139 mm in width. In order to obtain different confinements in both *x* and *z* direction (see Fig. 1 for axis reference), glass sheets and stripes were used. The sheets have the same width and height of the tank walls and their displacement inside the tank leads to a gap in the z direction (Fig. 1 (b)). In turn, the stripes were positioned perpendicular to the wall of the z gap, resulting in a confinement in the *x* direction (Fig. 1 (c)). Different configurations of distances in between the walls in both planes were achieved (3 mm to 12 mm. The resulting tank geometry was filled with deionized water at room temperature (ρ=997kg/m^3, σ=0.073N/m, μ=0.001Pa.s), which was used as the quiescent media. Air bubbles were injected manually at the bottom of the container by using a syringe and capillary tubes with distinct internal sizes. This configuration is depicted at the bottom of the Fig. 1 (a).

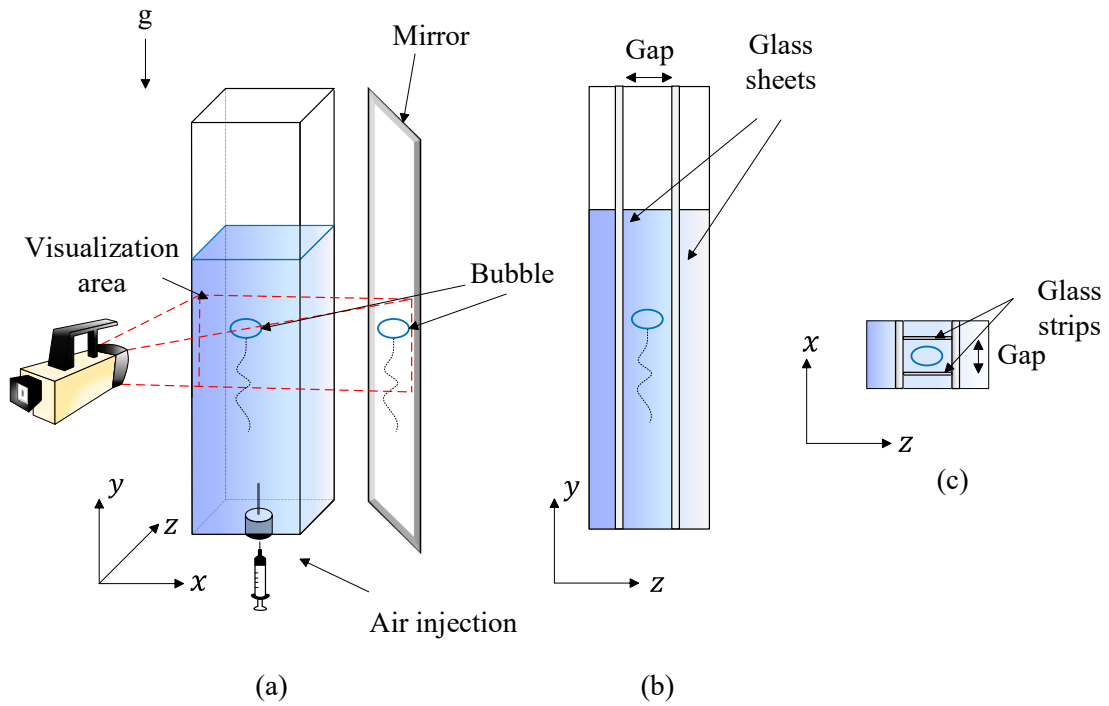

Figure 1-Schematic of the experimental setup: (a) general configuration, (b) y-z plan view and (c) x-z plan view

The obtained bubbles had diameters in the range of 1.32 to 3.06 mm and were categorized in three groups according to Tab. 1. The small ones have diameters ranging from 1.32 mm to 1.58 mm. In turn, when they have D varying between 2 mm to 2.50 mm, they are named medium. Lastly, when the measured D was found to be higher than 2.80 mm and lower than 3.10 mm they were referred as large. The combination of the channel geometries and bubble sizes studied in the present work, led to 30 different experimental configurations. Thus, the confinement parameter, defined as D/Dh, was varied from between 0.13 to 0.99. It is important to point out, that, in any of the studied cases, the bubbles were flattened by the walls of the channel.

A high-speed camera (FASTCAM SA4 model 500k-M3) was employed for image sequences capturing at an acquisition rate of 200 fps. The camera was located in front of the channel, while a mirror was placed at 45º relative to the tank wall (Fig. 1 (a)). In this manner, simultaneous images from the frontal and the lateral views of the bubble were acquired. The measurements were carried out at a distance of approximately 140 mm from the capillary tip; this was done in order to ensure that the bubbles reached their terminal velocity. The visualization window was of 140-mm in height and 174-mm in width and was illuminated by LED lights located both the back and lateral sides of the container. The recorded images were processed by applying several subroutines in a developed code in commercial software MATLAB®.

3. RESULTS

In this section are present the results of a study concerning the effects of the confinement direction over the shape, terminal velocity and drag coefficient of the single bubbles.

3.1 Bubble shape

Figure 2 shows the evolution of the aspect ratio for all the channels as a function of the confinement parameter (D/Dh). The overall effect of increasing D/Dh is to decrease bubble deformation. Sirino et al., 2021 attributed this behavior to the increases in shear stresses by the bubble-wall proximity. It is observed that, for confinement degrees higher than 0.5 (dash-dotted line), all the bubble sizes exhibit an aspect ratio smaller than 1.15, which indicates almost spherical bubbles. The change in the slope of the data with the same channel geometry shows that the increase in the confinement substantially affects the shapes of the large bubbles. Nonetheless, it is important to note that different aspect ratios exist for the same confinement degree. This indicates that the bubble shapes not only depend on the confinement degree; they also rely on the confinement direction. It is noted that the plane with the smaller distance between the walls is the preferable for the oscillatory motion. Thus, a reduction in the distance between the walls leads to larger oscillation frequencies. Hence, it is likely that even for channels with the same Dh, for rectangular geometries the shorter side would exhibit more bubble-wall interactions, thus reducing the mean bubble aspect ratio.

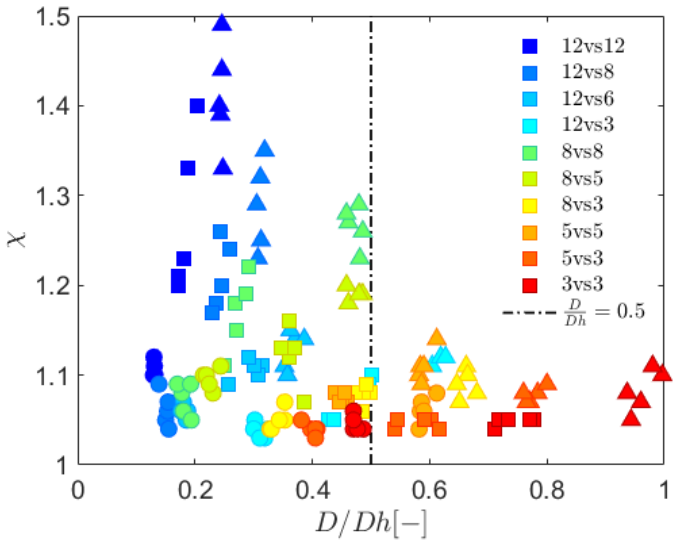

Figure 2- Aspect ratio as a function of the bubble confinement degree (D/D_h), the black dash-dotted line shows the $(D/D_h) = 0.5$ value. The symbols for the different bubble sets are as follows: ○ small bubbles, □ medium bubbles and △ large bubbles

The relation between the aspect ratio and the Weber number for the present results is shown in Fig. 3. For comparison purposes, the models of Moore, 1965 and Legendre et al., 2012 valid for unbounded systems are shown. The Moore, 1965 correlation was based upon the irrotational flow theory, which is valid for high Reynolds numbers and small aspect ratios.

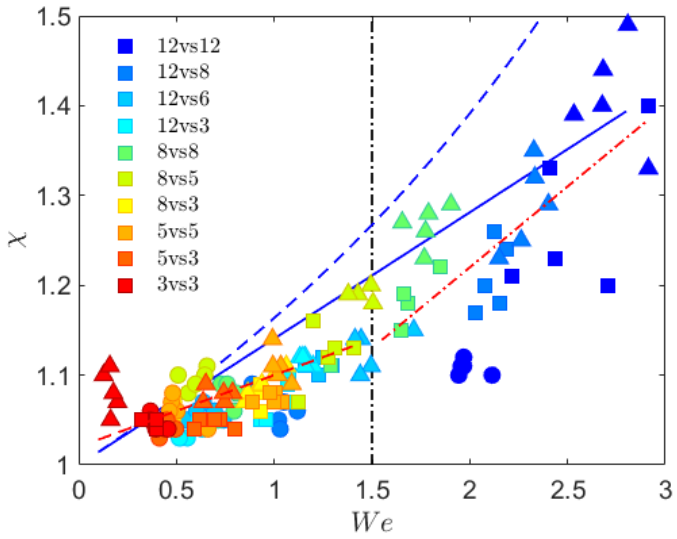

Figure 3- Aspect ratio versus the Weber number compared with models for non-confined systems. Continuous and dashed blue lines correspond to the Moore, 1965 and Legendre et al., 2012 correlations, respectively. Red dash-dotted lines correspond to the correlations proposed in the present study for We < 1.5 and We > 1.5. Black line represents the We = 1.5 limiting value. The symbols for the different bubble sets are as follows: ○ small bubbles, □ medium bubbles and △ large bubbles

On the other hand, the (Legendre et al., 2012) model is valid for pure water and aspect ratios smaller than 2.5, which are larger than those observed in this work. It is clearly noted that such models do not agree well with the present data, the correlation of (Moore, 1965) works better than (Legendre et al., 2012) equation since it predicts smaller deformations. Thus, correlations between the aspect ratios and the Weber numbers valid for the present system were proposed by means of experimental data fitting as:
For We < 1.5:

$$\chi = 0.08We + 1.02 \quad (1)$$

whereas for We > 1.5, the aspect ratio can be described by:

$$\chi = 0.08We^2 - 0.51We + 1.61 \quad (2)$$

3.2 Bubble velocities

The influence of the confinement direction in the behavior of the terminal velocity is shown in Fig. 4, where bubbles are binned as small (a), medium (b) and large (c) sizes, respectively. For the small bubbles (Fig. 4(a)) the earliest velocity decrease occurs for the 12x8-mm channel and Dh= 9.6 mm. Then, the velocities descend to a lower level at the 8x8-mm channel with Dh= 8 mm. It is observed that the 8-mm length is the limiting distance for the velocity decrease. The velocity differences between the 12x8-mm and 8x8-mm tanks occur because the 8x8mm is a symmetrical geometry and no preferential plane for bubble-wall interaction exists (helicoidal path). Hence, the bubbles undergo a double confinement effect by their interactions with the four walls (both directions). The velocities in the 12x6-, 12x3-, 8x5- and 5x5-mm channels, corresponding to Dh = 8, Dh = 4.8, Dh = 6.15 and Dh = 5, respectively, and remains in the same range.

Moreover, in Fig. 4(a), it must be pointed out that the 8x8- and 12x6-mm channels had the same hydraulic diameter and consequently the same confinement degree (D/Dh), but the bubbles show differences in their velocities. It can then be acknowledged that the hydraulic diameter is not the single criterion required to evaluate the confinement effect. Thus, it can be identified that the confinement orientation leads the bubble velocity. In consequence, the channel with the narrower distance between walls (6-mm) will present minor velocities. The side with the smaller gap corresponds to the preferential oscillatory plane. Thence, in the 6-mm gap a new limit distance where the small bubbles change their velocity range was identified. In the case of the 8x3-mm channel (Dh = 4.36) a further velocity decrease is observed, but bubbles flowing in the 5x3-mm and 3x3-mm channels remained in the same range. On the other hand, for the $4.36 \geq D_h \geq 3$ channels, the direction of confinement seems to not have any influence.

The medium bubbles, Fig. 4(b), showed a behavior similar to that observed for small bubbles in the 8-mm gap, as a critical distance where bubble velocity modulation begins. For the 12x8-mm and 8x8-mm channels, a declination in terminal velocity is noted. Moreover, the bubbles velocities for the 12x6-, 12x3-, 8x5-, 8x3- and 5x5-mm channels ($8 \geq D_h \geq 4.36$) remains in the same range. The behavior deviations between small and medium diameters correspond to the differences in the forces involved in the bubbles while they rise. Therefore, in the 8x3-mm channel (Dh = 4.36), the higher buoyancy of the medium bubbles is able to overcome the drag force generated into that channel. Similar shifts in velocities are noted for the 5x3-mm and for 3x3-mm channels as previously discussed.

Additionally, in Fig. 4(c), the large bubbles also presented a velocity-decaying trend, in a fashion similar to that observed for the small and medium bubbles up to the 12x8-mm channel. Obviously, the large bubbles have higher buoyancy forces than the smaller bubbles previously analyzed. Such a force can easily overcome the drag forces induced in more confined channels. In addition, the bubble velocities for the 12x6-, 8x8- and 8x5-mm, corresponding to $8 \geq D_h \geq 6.15$, are in the same range. For the large bubbles, the 5x5-mm channel imposes a severe confinement that keeps the velocities in the same level as the 12x3- and 8x3-mm channels ($D_h \simeq 5$). For the other vessel sizes (5x3-mm, 3x3-mm) a continuous linear decrease in the velocities is observed. From the above analysis, it can be seen that for the force balance in rectangular channels, the bubble size and the confinement direction must be taken into account since the flow induced by the bubble passage is strongly influenced by both the bubble-to-walls proximity and the corners of the channels. Furthermore, as was shown before, the geometry of the tanks largely affects the dynamics of the bubbles.

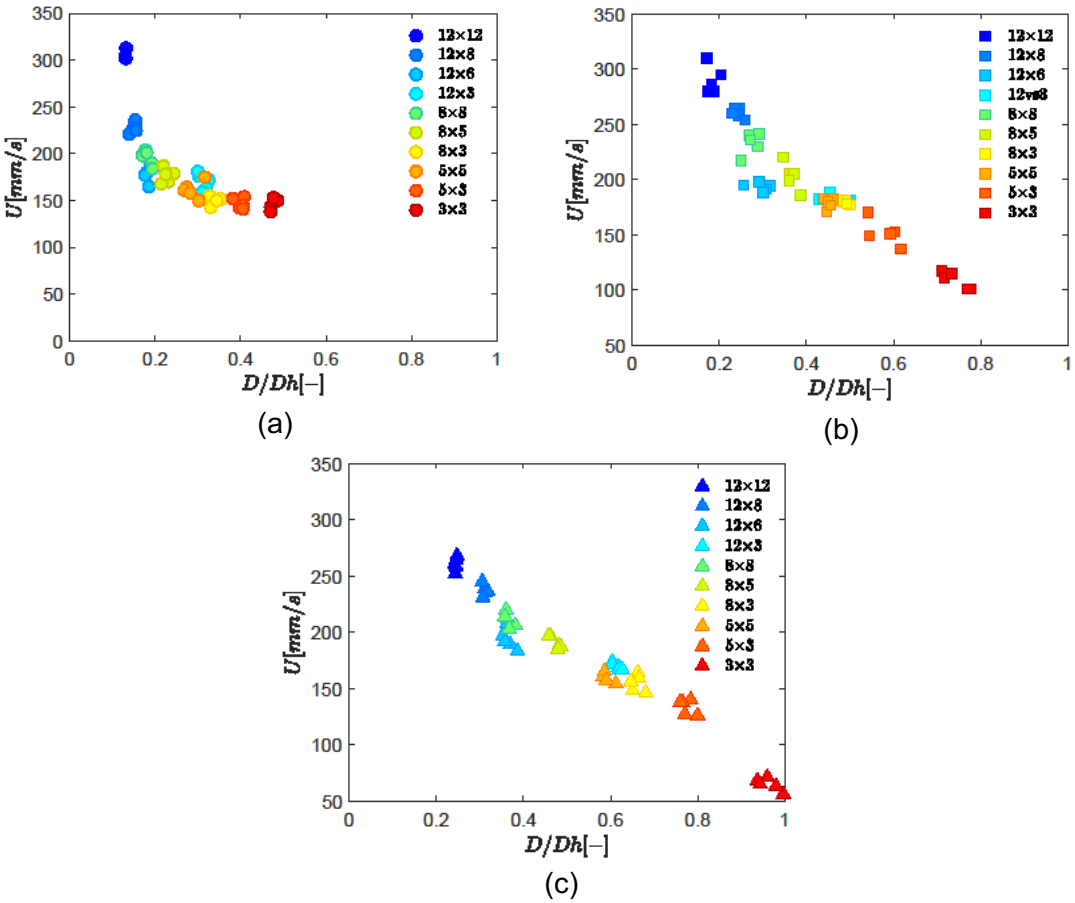

Figure 4-Terminal velocities as a function of the confinement parameter for the different bubble sizes and geometrical configurations. (a) ○ small bubbles, (b) □ medium bubbles and (c) △ large bubbles.

3.3 Drag coefficient

The resistance to the flow of the bubbles could be estimated by the drag coefficient, which can be obtained by the balance between the drag and buoyancy forces as:

$$Cd = \frac{4Dg}{3U^2} \tag{3}$$

Figure 5 shows the evolution of the drag coefficient as a function of the confinement parameter. The drag coefficient increases with the increase of the D/Dh parameter, which implies small Dh values. For the large bubbles in the 3x3-mm channel, the drag coefficients are around four times higher than the ones found for the medium bubbles rising in the same configuration. Several drag coefficients valid for bubbles rising freely in stagnant liquid have been proposed over the years, such as in Ishii and Chawla (1979), Mei (1994), Tomiyama et al. (1998), Dijkhuizen et al. (2010). These were usually developed for spherical bubbles, which follow rectilinear trajectories, where the viscous forces are dominant and the drag coefficients are based on the Reynolds number. On the other hand, for deformed bubbles, where oscillatory paths are observed, the surface tension gains importance, and the models contemplate the Eötvös number. Recently, a model for the drag coefficient of bubbles rising through a non-confined system was presented by Yan et al., 2017. This model was based on the Schiller-Naumann correlation and data fitting for deionized water at 550 < Re <1700. Such a correlation uses Re, Eo and We numbers and considers the instantaneous velocities of the bubbles. For the sake of comparison, the current results are plotted against the model by Yan for the Cd in Fig. 5b. Interestingly, this model shows a good agreement with all the present cases, being the largest deviations (< 5 %) for the small bubbles in the 3x3-mm channel. The origin of these slight deviations could be explained by the oscillatory trajectories of these bubbles, meaning a drag increase that is not observed in an unconfined system. Overall, the aforementioned concordance is possibly because the Schiller-Naumann model is valid for spherical bubbles, as well as the present cases, where small deformations are observed.

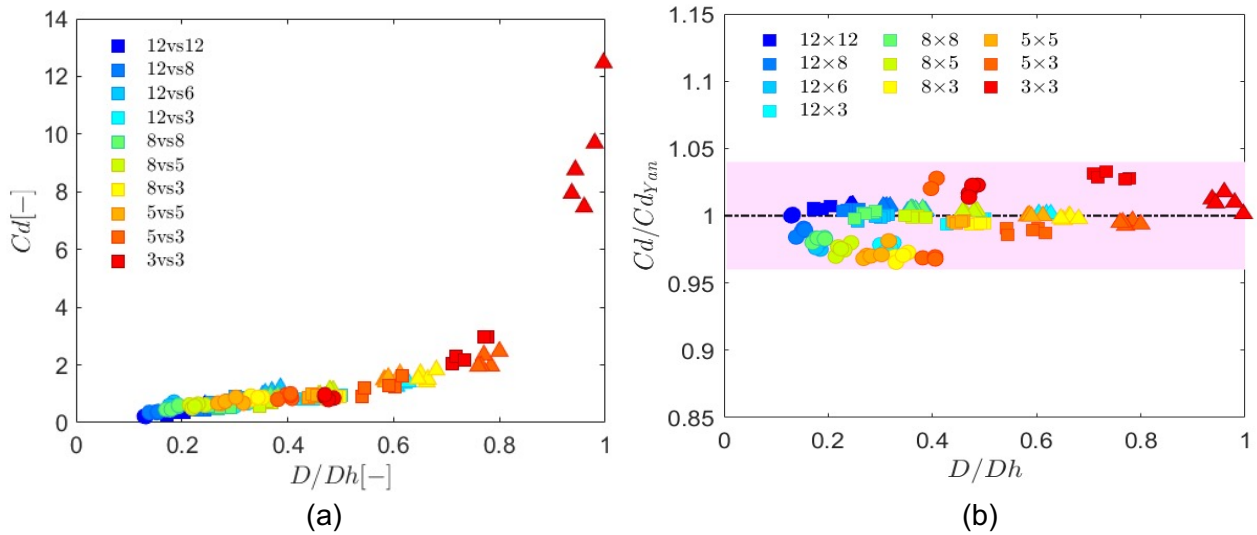

Figure 5-(a) Drag coefficient as a function of (D/D_h), (b) ratio of calculated drag coefficient to (Yan et al., 2017) model. The symbols for the different bubble sets are as follows: ○ small bubbles, □ medium bubbles and △ large bubbles.

Furthermore, in confined systems many other factors determine the magnitude of the drag forces, which are expected to be larger than the ones found in unrestricted systems. In this regard, (Figueroa-Espinoza et al., 2008) pointed out that energy losses by the collisions of the bubbles against the walls, high vorticity production and viscous dissipation by the liquid film around the bubbles are responsible for increasing the drag coefficient. Alternatively, by taking as a base the (Levich, 1949) model for the drag coefficient, which is based on the boundary layer theory, it is possible to introduce additional effects. The influence of the bubble shape, drag force by confinement and vorticity production can be included by incorporating the Eötvös number and the geometric parameter (D/D_h) to the model. This relation is presented in Fig. 6. It was disregarded for the large bubbles in the 3x3-mm channel because of the differences in the drag values for the other cases as it can be seen in Fig. 5(a).

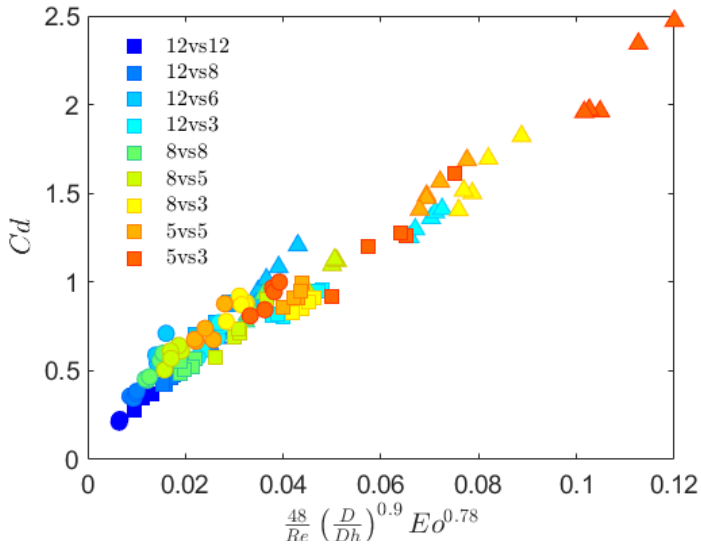

Figure 6- Drag coefficient as a function of the confinement parameter (D/D_h) and Reynolds and Eötvös numbers. The continuous black line shows the drag coefficient model proposed (Eq.10). The symbols for the different bubble sets are as follows: ○ small bubbles, □ medium bubbles and △ large bubbles

As the confinement degree (D/D_h) increases, the bubble velocity and aspect ratio decrease, hence the growing linear trend of the drag coefficient (Fig. 19) can be computed with a good agreement as:

$$Cd = 0.21 + 17.78\left[\frac{48}{Re}\left(\frac{D}{D_h}\right)^{0.9} Eo^{0.78}\right] \quad (4)$$

The presented correlation is valid for $0.13 < D/D_h < 0.7$.

4. ACKNOWLEDGEMENTS

PETROBRAS

5. REFERENCES

Böhm, L., Kurita, T., Kimura, K., Kraume, M., 2014. "Rising behaviour of single bubbles in narrow rectangular channels in Newtonian and non-Newtonian liquids". *International Journal of Multiphase Flow,* Vol. 65, pp. 11–23.

Cano-Lozano, J., Bohorquez, P., Martínez-Bazán, C., 2013. "Wake instability of a fixed axisymmetric bubble of realistic shape". *International Journal of Multiphase Flow,* Vol. 51, pp. 11–21.

Cano-Lozano, J.C., Martínez-Bazán, C., Magnaudet, J., Tchoufag, J., 2016. "Paths and wakes of deformable nearly spheroidal rising bubbles close to the transition to path instability". *Physical Review Fluids, Vol.* 1, 053604.

Celata, G.P., D'Annibale, F., Di Marco, P., Memoli, G., Tomiyama, A., 2007. "Measurements of rising velocity of a small bubble in a stagnant fluid in one and two-component systems". *Experimental Thermal and Fluid Science,* Vol. 31, pp. 609–623.

Dijkhuizen, W., Roghair, I., Annaland, M.V.S., Kuipers, J., 2010. "DNS of gas bubbles behaviour using an improved 3D front-tracking model—drag force on isolated bubbles and comparison with experiments". *Chemical Engineering Science*, Vol. 65, pp. 1415–1426.

Drews, A., Prieske, H., Meyer, E.L., Senger, G., Kraume, M., 2010. "Advantageous and detrimental effects of air sparging in membrane filtration: Bubble movement, exerted shear and particle classification". *Desalination, Vol.* 250, pp. 1083– 1086.

Figueroa-Espinoza, B., Zenit, R., Legendre, D., 2008. "The effect of confinement on the motion of a single clean bubble". *Journal of Fluid Mechanics*, Vol. 616, pp. 419– 443.

Filella, A., Ern, P., Roig, V., 2015. "Oscillatory motion and wake of a bubble rising in a thin-gap cell". *Journal of Fluid Mechanics*, Vol. 778, pp. 60–88.

Ishii, M., Chawla, T., 1979. "Local drag laws in dispersed two-phase flow". *ANL-79-105, Argonne National Laboratory. Technical Report N* 80, 25631.

Kumar, P., Vanka, S.P., 2015. "Effects of confinement on bubble dynamics in a square duct". *International Journal of Multiphase Flow*, Vol. 77, pp. 32–47.

Legendre, D., Zenit, R., Velez-Cordero, J.R., 2012. "On the deformation of gas bubbles in liquids". *Physics of Fluids*, Vol. 24, 043303.

Levich, V., 1949. "The motion of bubbles at high Reynolds numbers. Zh. Eksp". *Teor. Fiz,* Vol. 19, 436ff.

Mei, R., 1994. "Flow due to an oscillating sphere and an expression for unsteady drag on the sphere at finite Reynolds number". *Journal of Fluid Mechanics*, Vol. 270, pp. 133–174.

Moore, D., 1965. "The velocity of rise of distorted gas bubbles in a liquid of small viscosity. Journal of Fluid Mechanics", Vol. 23, pp. 749–766.

Premlata, A., Tripathi, M.K., Sahu, K.C., 2015. "Dynamics of rising bubble inside a viscosity-stratified medium*". Physics of Fluids*, Vol. 27, 072105.

Sharaf, D., Premlata, A., Tripathi, M.K., Karri, B., Sahu, K.C., 2017. "Shapes and paths of an air bubble rising in quiescent liquids". *Physics of Fluids,* Vol. 29, 122104.

Sirino, T., Mancilla, E., Morales, R.E., 2021. "Experimental study on the behavior of single rising bubbles in a confined rectangular channel". *International Journal of Multiphase Flow,* Vol. 145, 103818.

Soltani, H., Sabbagh, R., Nobes, D.S., 2018. "The passage of bubbles rising through a confining rectangular geometry". *Physics of Fluids*, Vol.30, 103302.

Tomiyama, A., Celata, G., Hosokawa, S., Yoshida, S., 2002. "Terminal velocity of single bubbles in surface tension force dominant regime". *International Journal of Multiphase Flow,* Vol. 28, pp. 1497–1519.

Tomiyama, A., Kataoka, I., Zun, I., Sakaguchi, T., 1998. "Drag coefficients of single bubbles under normal and micro gravity conditions". *JSME International Journal Series B Fluids and Thermal Engineering*, Vol.41, pp. 472–479.

Tripathi, M.K., Sahu, K.C., Govindarajan, R., 2015. "Dynamics of an initially spherical bubble rising in quiescent liquid". *Nature Communications,* Vol. 6, pp. 1–9.

Yan, X., Jia, Y., Wang, L., Cao, Y., 2017. "Drag coefficient fluctuation prediction of a single bubble rising in water". *Chemical Engineering Journal*, Vol. 316, pp. 553–562.